TECHNICAL REPORT STANDARD PAGE

1. Title and Subtitle
   Investigation of Free-Standing Polymer Composites for Robotic-Driven Bridge Construction
2. Author(s)
   Genevieve Palardy (PI) & Corina Barbalata (Co-PI)
3. Performing Organization Name and Address
   Department of Mechanical & Industrial Engineering
   Louisiana State University
   Baton Rouge LA, 70803
4. Sponsoring Agency Name and Address
   Louisiana Department of Transportation and Development
   P.O. Box 94245
   Baton Rouge, LA 70804-9245
5. Report No.
   FHWA/LA.24/24-1TIRE
6. Report Date
   July 2024
7. Performing Organization Code
   LTRC Project Number: 24-1TIRE
   SIO Number: DOTLT1000496
8. Type of Report and Period Covered
   Final Report
   7/2023 – 6/2024
9. No. of Pages
   40
10. Supplementary Notes
    Conducted in Cooperation with the U.S. Department of Transportation, Federal Highway Administration.
11. Distribution Statement
    Unrestricted. This document is available through the National Technical Information Service, Springfield, VA 21161.
12. Key Words
    Additive manufacturing, photopolymer composites, frontal polymerization, robotic system
13. Abstract

The overall objective is to conduct preliminary research to enable free-standing 3D printing of bridge structures with fiber-reinforced polymers and robotic systems. Two material systems were considered: 1) frontal polymerization (FP) epoxy-vinyl ether composites and 2) photopolymer reinforced with fumed silica and/or glass fibers. For the FP resin, a formulation containing 4 wt% fumed silica and carbon nanofibers was the most suitable for free-standing printing, demonstrated via angled filaments and helixes. Flexural properties showed specimens printed in the transverse direction exhibited the lowest strength, likely due to voids within and between filaments. For glass fiber-reinforced photopolymers, a robotic 3D printing system was designed with a custom extruder end-effector to facilitate in-situ impregnation of fibers and resin. Free-standing angled filaments and planar, cylindrical specimens were successfully printed to assess quality and curing capabilities without the use of supports. Overall, potential for free-standing printing of composite structures was demonstrated with the robotic system, which can be leveraged for various bridge truss geometries.

Project Review Committee

Each research project will have an advisory committee appointed by the LTRC Director. The Project Review Committee is responsible for assisting the LTRC Administrator or Manager in the development of acceptable research problem statements, requests for proposals, review of research proposals, oversight of approved research projects, and implementation of findings.

LTRC appreciates the dedication of the following Project Review Committee Members in guiding this research study to fruition.

LTRC Administrator/Manager

Vijaya Gopu, PhD, P.E.

Directorate Implementation Sponsor

Chad Winchester, P.E.

DOTD Chief Engineer

Investigation of Free-Standing Polymer Composites for Robotic-Driven Bridge Construction

By
Genevieve Palardy, PhD, PI
Corina Barbalata, PhD, Co-PI

Department of Mechanical & Industrial Engineering
Louisiana State University
Baton Rouge LA, 70803

LTRC Project No. 24-1TIRE
SIO No. DOTLT1000496

conducted for
Louisiana Department of Transportation and Development
Louisiana Transportation Research Center

July 2024

Abstract

The overall objective of this project is to conduct preliminary research to enable free-standing 3D printing of bridge structures with fiber-reinforced polymers and robotic systems. Two material systems were considered: 1) frontal polymerization (FP) epoxy-vinyl ether composites and 2) photopolymer reinforced with fumed silica and/or glass fibers. The following tasks were achieved: (A) study the relationship between material properties and 3D printing parameters with small-scale benchtop systems and (B) Investigate free-standing 3D printing using fiber-reinforced polymers with benchtop or robotic arm systems. Most studies were performed on a benchtop 3D printing system with preliminary free-standing experiments run on a robotic arm system to identify challenges and limitations moving forward. For the FP resin system, a formulation containing 4 wt% fumed silica and 4 wt% carbon nanofibers was the most suitable for free-standing printing, demonstrated via angled filaments and helixes. Flexural properties showed specimens printed in the transverse direction exhibited the lowest strength, likely due to voids within and between filaments, adhesion issues, and preferential carbon nanofiber alignment along the filaments. For glass fiber-reinforced photopolymers, a robotic 3D printing system was designed and manufactured with a custom extruder end-effector to facilitate free-standing printing of complex geometries. In this case, continuous GF tows were combined with the photopolymer via an in-situ impregnation chamber in the end-effector to produce filaments and structures with higher strength and stiffness. Free-standing angled filaments and planar, cylindrical specimens were successfully printed to assess quality and curing capabilities without the use of supports. Overall, potential for free-standing printing of composite structures was demonstrated with the robotic system, which can be leveraged for various bridge truss geometries.

Acknowledgements

The authors would like to acknowledge Mark Brennan and Roger Greene for their assistance during mechanical testing and setup of the robotic 3D printing system in the LSU Mechanical Engineering machine shop. Drs. John Pojman and Brecklyn Groce from the Department of Chemistry at LSU are gratefully acknowledged for providing frontal polymerization formulations throughout this project.

Some outcomes from this work were partially sponsored by the National Science Foundation under Grant 2051050 (REU SMART Polymers), and the US National Science Foundation under Grant OIA-1946231 and the Louisiana Board of Regents for the Louisiana Materials Design Alliance (LAMDA).

Implementation Statement

While this work is exploratory and would require further research before its direct implementation on bridge structures is carried out, findings for small-scale specimens allow general identification and development of manufacturing/processing procedures. Those include desirable material properties and additive manufacturing parameters, such as polymer composite system, viscosity, filler or fiber weight fraction, extrusion pressure and speed, printing speed, and cure initiation mechanisms. Those material characteristics and printing parameters can directly be translated from desktop to robotic 3D printing system, reducing the need for experimental trials. As a next step, those findings would be tested on larger scale structures, such as bridge components, and material characterization and testing results would be implemented into finite element models to support future design endeavors.

Table of Contents

List of Figures

Introduction

Deterioration of bridges is a recognizable problem worldwide. In 2022, out of 12,733 bridges in the State of Louisiana, over 1,500 bridges were classified as structurally deficient (poor performance), according to the National Bridge Inventory [1]. The majority of those bridges are made of concrete, steel or wood. Fiber-reinforced polymers (FRPs) are a promising alternative to conventional materials as they are corrosion resistant, structurally durable, lightweight, require less maintenance, and possess low moisture absorption, as well as better load-carrying capability (because of their high strength- and stiffness-to-weight ratios) [2]. Moreover, their low weight can reduce installation time and transportation cost. This makes them well-suited for several types of bridges, including footbridges and movable bridges, a common sight in Southern Louisiana [3]. Therefore, they have been considered for bridge construction and for repair/strengthening of existing structures [2, 4]. To address the rise of FRP in bridge construction, the American Association of State Highway and Transportation Officials (AASHTO) dedicated a standard covering requirements for FRP composite material systems intended for use in bridge and highway structures [5].

However, large-scale fabrication is challenging and potentially costly. Additive manufacturing (AM), or 3D printing, is a promising technique that allows segmental fabrication of large structures and shows potential for free-standing printing (no supports). The latter can potentially be achieved with photopolymers (thermoset resins) or frontal polymerization resins, as their solidification (cure) is initiated right after extrusion through ultraviolet (UV) light or localized heat source [6-8]. In combination with mobile robotic manipulators that allow for complex movements, on-site manufacturing could be achieved, further decreasing transportation costs. Free-standing AM with FRPs and robotic systems is still in the early stages of research and therefore, further investigation is needed to assess its feasibility. The proposed research will explore untested and novel ideas in this emerging field to potentially enhance and complement traditional bridge fabrication and construction 3D printing.

Literature Review

In terms of large-scale bridge structures, the literature is mostly focused on metal, concrete, or thermoplastic materials, but not specifically on FRPs. Figure 1 shows examples of 3D printed bridges made from conventional materials, like steel (Figure 1a) and thermoplastic (Figure 1b) [9]. The former was printed by MX3D (Amsterdam, The Netherlands) utilizing robotic wire arc additive manufacturing (WAAM). The latter was manufactured via a robotic system similar to fused deposition modeling at the University of Shanghai. The vast majority of such projects are conducted via industry to demonstrate software and custom capabilities, but manufacturing systems are not directly commercially available to potentially study the use of new materials.

Figure 1. Examples of 3D printed bridges

(a) MX3D free-form printing of steel bridge (artist's rendition) [9]

(b) Thermoplastic 3D printed bridge with Kuka robotic arm (Source: University of Shanghai, China)

Aside from the materials listed above, FRPs have attracted attention in 3D printing because of the high specific stiffness and strength. In particular, free-standing (or free-form) printing is promising because it would reduce waste (no need for material supports), manufacturing time, and cost. Photopolymers and frontal polymerization (FP) resins are good candidates to enable such a technology because they are thermosets that can be solidified as they are deposited [6-8]. UV curing, implemented with extrusion-based printing methods (like direct ink writing, DIW), is a promising approach for free-standing printing of thermoset polymers. Its free-form capabilities were demonstrated with modified desktop printers or gantry systems [8, 10-14] and custom-designed 5-axis systems [15]. The extruder head designs typically include micro-pumps, syringe pumps, or pneumatic regulators to deliver resin to the nozzle, and multiple laser diodes to cure

resin as it is extruded. AM of continuous fiber-reinforced UV-curable thermosets has also been investigated through desktop systems equipped with a dispensing syringe fitted with a pneumatic regulator [16-17]. In industry, companies such as Continuous Composites, Inc. (USA) and Moi Composites (Italy), have demonstrated AM of continuous fiber-reinforced UV-curable thermosets with robotic manipulators and custom-designed printing heads. However, those systems and end-effector extruders are not readily commercially available at affordable costs for development with new materials. Consequently, research in this field is limited. To partially address this shortcoming, previous work from the PI and Co-PI achieved design and development of a robotic 3D printer system for UV-curable thermosets with a low-cost end-effector [18-19].

Frontal polymerization (FP) is a process wherein an initial stimulus initiates a localized polymerization reaction that propagates through uncured resin, curing the resin as it travels. The process relies on heat diffusion and Arrhenius rate kinetics of an exothermic reaction [20-22]. Radical-induced cationic frontal polymerization (RICFP) allows for FP of epoxies and vinyl ethers, high strength polymer matrices commonly used in FRPs, through the combination of a thermal radical initiator that promotes decomposition of a superacid generating salt [23-24]. It can be initiated by either heat or UV light.

The use of FP for 3D printing has advantages in energy consumption and speed of printing. An ideal process will see that the front is initiated and propagates behind the extruded material very closely so that the resin does not sag, owing to suitable viscosity, and the front is continuous. There are a few reports of RICFP used for 3D printing. Zhang et al. investigated printing a formulation containing a commercial bisphenol A diglycidyl ether (BADGE)-based epoxy resin with an iodonium aluminate salt and benzopinacol initiating system [25]. They compared continuous carbon fiber (CF) tows, carbon nanotubes (CNTs), short CFs, and graphene oxide as reinforcements [26-28]. Formulations with the CNTs and continuous CF tows resulted in improved mechanical properties. CNTs are fillers with high thermal diffusion and have a much smaller diameter than carbon fibers with a higher specific surface area. Using the same resin, they found that 1 wt% CNTs or 1 wt% discontinuous CFs gave small increases in front velocity compared to the neat resin, while 1 wt% graphene oxide reduced the front velocity.

Overall, both photopolymers and FP resins present advantages and disadvantages for 3D printing, which need to be further investigated for free-standing structures. Photopolymers can sustain higher printing speeds, but may not reach full cure during extrusion, while FP systems are fully cured, but require low printing speeds and may be

costly or possess low mechanical performance unless reinforced with fibers [32]. In this project, we intend to demonstrate the potential of printing free-standing structures using two material systems to further understand limitations and develop adequate manufacturing procedures: 1) a photopolymer reinforced with fumed silica and/or glass fibers, and 2) FP epoxy-vinyl ether composites. Vinyl ethers were previously shown to increase reactivity when added to epoxy systems [24]. By using a vinyl ether in tandem with two different epoxies, we aim to formulate a reactive system with desirable rheological properties for extrusion-based 3D printing.

Objective

The overall objective of this project was to conduct *preliminary research to enable free-standing 3D printing of bridge structures with fiber-reinforced polymers and robotic systems*. To meet this objective, the following tasks were achieved: (A) Study the relationship between material properties and 3D printing parameters with small-scale benchtop systems and (B) Investigate free-standing 3D printing using fiber-reinforced polymers with benchtop or robotic arm systems. Two material systems were considered: 1) FP epoxy-vinyl ether composites and 2) a photopolymer reinforced with fumed silica and/or glass fibers. The outcomes will allow identification of suitable process parameters for robotic systems leading to high quality/performance.

Scope

The research was limited to photopolymers and frontal polymerization resins reinforced with fillers, short fibers, or continuous fibers. It aims to investigate the effect of processing parameters on printed specimens' quality (dimensions and/or mechanical performance) and/or free-standing potential to select promising material formulations for follow-up, in-depth studies. Most studies were performed on a benchtop 3D printing system with preliminary experiments run on a robotic arm system to identify challenges and limitations moving forward.

Methodology

Materials

The FP resin formulation contained the following chemicals (structures shown in Figure 2): 2,2-Bis(4-glycidyloxyphenyl)propane (Bisphenol A diglycidyl ether, BADGE) (TCI Chemicals), 3,4-epoxycyclohexylmethyl-3,4-epoxycyclohexanecarboxylate (CE) (Ambeed Inc.), tri(ethylene glycol) divinyl ether (TEGDVE) and 1,1-Bis(tert-butylperoxy)-3,3,5-trimethylcyclohexane (Luperox 231) (Sigma Aldrich), and p-(octyloxyphenyl)(phenyl)iodonium hexafluoroantimonate (IOC-8) (Hampford Research Inc.). Aerosil® 200 fumed silica (FS) was used as a filler to increase viscosity for printability (Evonik). PR-19-XT-HHT carbon nanofibers (CNFs) (Pyrograf Inc.) were used as a reinforcing constituent.

Figure 2. Structures of monomers and initiators used in printing resin [29]

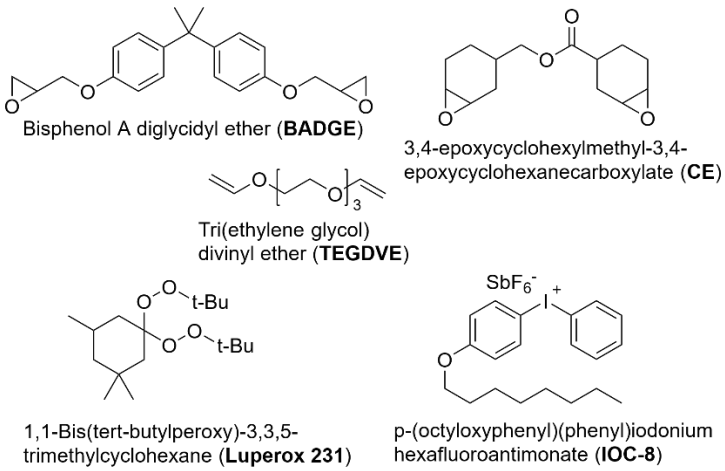

For studies with photopolymers, a commercially-available acrylic-based photopolymer was purchased (Anycubic). It has an UV wavelength between 365 nm and 410 nm. As viscosity was expected to influence the printed specimens' dimensional stability, fumed silica (FS, AEROSIL R972, from VWR), a common filler to modify viscosity of polymers, was incorporated into the resin. Continuous glass fiber (GF) rovings were purchased from Fibre Glast Corporation to reinforce the photopolymer during the robotic 3D printing process. GFs were chosen because UV light can pass through, whereas

carbon fibers (which possess higher strength and stiffness) block UV light and limit solidification of the photopolymer matrix through the thickness.

Preparation of Formulations

The FP resin was comprised of a mixture of 60 wt% BADGE, 20 wt% CE, and 20 wt% TEGDVE. To prepare formulations for frontal polymerization, first, IOC-8 was dissolved in a mixture of BADGE and CE using a heated sonicator at approximately 40°C. After dissolution, TEGDVE and Luperox 231 were added, and the mixture was stirred for 10 minutes using a high shear mixer with propeller. The IOC-8 acts as a superacid generator, while the Luperox 231 acts as a thermal radical initiator that produces radicals that induce decomposition of the IOC-8. For the fillers, FS was added and then the formulation was mixed in a FlackTek speed mixer at 800 rpm for 2 minutes. Then, CNFs were added and the formulation was mixed once at 900 rpm for 1 minute followed by two cycles at 1800 rpm for 3 minutes.

For the photopolymer, the resin was mixed with FS with a sonicator for 5 minutes. A weight fraction of 8 wt% was added for 3D printing with pure photopolymer. For GF-reinforced photopolymer, a weight fraction of 4 wt% was added.

Rheological Characterization

A parallel plate Discovery Hybrid Rheometer 20 (DHR-20, Waters TA Instruments) was employed to measure shear viscosity for resin formulations containing different FS and CNF weight fractions (0 wt% to 6 wt%). Resin samples were tested at 25°C with 25 mm diameter parallel plates in shear rate sweep mode from 0.1 to 100 s^{-1}. This data was used to study the shear thinning behavior of the polymer and establish which resin formulations would be suitable for free-standing 3D printing at room temperature. The main goal was to achieve a viscosity allowing consistent extrusion through the extruder nozzle, while avoiding sagging of the extruded material at the nozzle tip.

Extrusion-Based Additive Manufacturing Setups

Two extrusion-based AM setups were considered for this study (Figure 3). To investigate the behavior of the FP and photopolymer resins at a small-scale, a desktop 3D printer was modified and used as the main AM setup in this study (Figure 3a). An Ender-3 V2 3D printer was modified by replacing its heated fused deposition extruding unit with a custom-made syringe holder. The latter was 3D printed with polylactic acid and designed to hold a 10 ml syringe as an extruder. To obtain material flow, a tubing system was employed, connecting the syringe to a pressure controller. For regulating the pressure, a syringe dispenser (LOCTITE® digital syringe dispenser, Henkel) was utilized, able to adjust pressure within a range of 0 to 0.7 MPa (0 to 7 bar). A nozzle was attached at the tip of the syringe and its inner diameter measured 2 mm, unless specified otherwise. The printing platform maintained an average temperature of 25 °C. The process involved depositing the resin onto the platform, followed by a quick thermal initiation via two SkyBeam UV spotlights at 100 % intensity (10 W, 365 nm wavelength, 6 mm lens, 5.6 W cm^{-2} at a distance of 13 mm, UVitron International).

The modified 3D printing setup was first used to study the extrusion behavior of the FP resin as it represented the biggest challenge to find a suitable combination of printing parameters. To enable free-standing printing, the resin must be viscous enough to limit sagging as it is extruded, and the nozzle speed must be coordinated with the front speed to obtain solidification close to the tip while avoiding clogging. Printing with FP resin was studied with different filler weight fractions (FS and CNFs), under different pressures (0.02 to 0.15 MPa), nozzle diameters (1.5 and 2.0 mm), and printing speeds (1.5 cm min^{-1} to 6 cm min^{-1} or 0.25 mm s^{-1} to 1.0 mm s^{-1}). Videos of the extrusion at the nozzle were captured, and deposited filaments width and thickness were measured with a caliper to find a suitable set of parameters based on resin formulation. The main goal was to find filler weight fraction, pressure, diameter, and printing speed combinations to achieve consistent material extrusion, while avoiding material sagging at the nozzle exit to enable free-standing printing. Once a formulation was selected, planar specimens were printed for mechanical characterization. Free-standing printing was then demonstrated with single filaments printed at an angle (40º) and helical geometries. Sample geometries were modeled in SolidWorks, then imported in UltiMaker Cura 5.4 as .stl files and saved as .gcode files for the printing process. For free-standing printing, gcode files were manually modified to produce single paths.

While studies with the desktop 3D printer were conducted, a robotic setup with a Kuka KR 300 R2700 manipulator and custom-designed end-effector was manufactured and tested as part of a Capstone Design project (Figure 3b, Figure 3c, and Figure 3d). Due to the complexity of the setup and time limitations for this project, only fiber-reinforced photopolymer printing was tested with this system. The AM system contains seven main sub-systems, in addition to the Kuka arm: 1) power supply for the arm, controller, and end-effector components, 2) PLC to drive the robotic arm, stepper motor, UV lights, and peristaltic pump supplying the resin, 3) resin storage and supply (compatible with a wide range of thermosets), 4) continuous fiber storage and supply (Figure 3c), 5) continuous fiber filament impregnation site (Figure 3d), 6) extruder nozzle (Figure 3d), and 7) UV lighting (Figure 3d). The resin supply line controls the flow of resin from the storage location on top of the Kuka arm to the end-effector. A peristaltic pump achieves the desired flow rate and delivers it to the end-effector through a resin feed line. This line is split to provide resin flow to both sides of the impregnation chamber through the inlets. The fiber supply system is mounted between the fiber storage location and the outlet of the end-effector. The impregnation chamber's main purpose is to allow both resin and fiber reinforcement to meet at one place in the feed and leave together at the same speed. The resin enters on the other end of the chamber to ensure that there is minimal pressure of the resin inlet valve. Finally, the UV lighting sub-system consists of 4 UV LEDs positioned in a ring configuration around the extruder nozzle, and housed in an aluminum lens tube equipped with an aspheric condensing lens. The intensity output of each light is controllable on the dimming accessory board, and analog signals can be used to scale the knob-set maximum intensities of the LED channels.

Initial 3D printing tests at constant pump speed (between 2.5% and 15%), roller tension, UV light intensity (75%), and arm velocity were performed with glass fiber (GF) tows and a commercially-available photopolymer. A metal nozzle with a diameter of 1.5 mm was employed. Planar specimens (e.g., cylindrical geometries with 10 cm diameter) and free-standing angled filaments were printed to assess impregnation quality and curing capabilities without the use of supports, but no mechanical testing was performed so far.

Figure 3. AM setups designed and used for this study

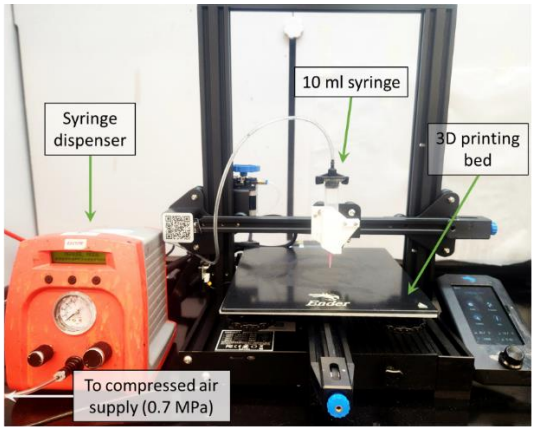

(a) Modified 3D printing setup for small-scale study with FP and photopolymer resins. A syringe dispenser was used to control the flow of the resin into a 10 mL syringe.

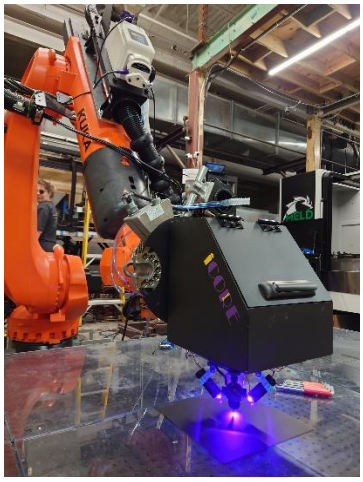

(b) Robotic 3D printing system for fiber-reinforced photopolymers: Kuka robotic arm with custom-designed end-effector. The setup was completed and tested during this project.

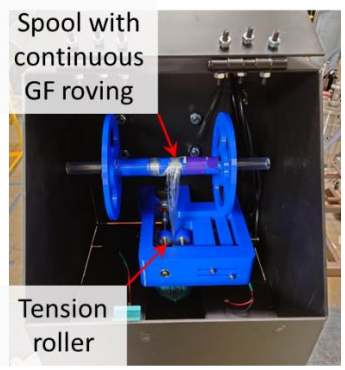

(c) Internal view of robotic end-effector components showing GF spool and tension mechanism with roller.

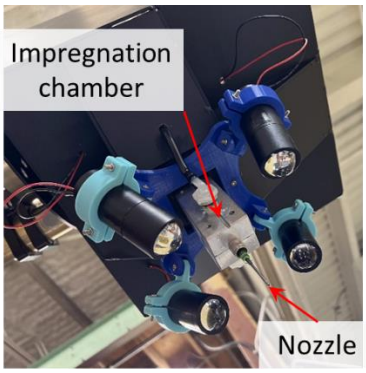

(d) Bottom view of robotic end-effector components showing impregnation chamber and nozzle.

Mechanical Performance Characterization

Mechanical testing was performed on FP resin specimens. As new FP formulations were 3D printed, it was judged important to assess their mechanical performance, while the photopolymer used in this project was commercially available and already contained mechanical testing data in the literature.

Tensile tests were performed with a 50 kN test machine (TestResources 313) on molded specimens for different FP resin formulations to assess the effect of filler content (fumed silica and carbon nanofibers). Dogbone specimens were molded with a 3-part acrylic mold, based on ASTM D638 Type V geometry, as shown in Figure 4a. The specimens were lightly sanded before testing to remove sharp edges or surface defects. For tensile testing, the specimens were clamped with hydraulic grips and an extensometer (E3442, 50.8 mm gage, Epsilon Technology Corp.) was positioned on each sample to acquire displacement data under a loading rate of 1.3 mm min^{-1} (Figure 4c). Each experiment was carried out on six to eight molded specimens (n = 6 to 8) for each resin formulation. Ultimate strength, elastic modulus, and strain at break were obtained from the stress-strain curves, as well as their corresponding standard deviations. To remove any outliers, the Chauvenet's Criterion method was used when analyzing all data.

To compare mechanical performance between molded and 3D printed specimens, a rectangular 3-point bending (3PB) geometry was employed based on ASTM D790. It allowed 3D printing of specimens in the longitudinal and transverse directions (shown in Figure 4d) to evaluate the effect of filament orientation on mechanical performance under bending. Rectangular specimens were molded with a 3-part acrylic mold as shown in Figure 4b. It was coated with a release agent, then the resin was poured into the mold, pressed with a top acrylic plate, and the reaction was started with a soldering iron at a temperature of 200℃ at one end of the sample. Rectangular specimens had a base length of 65 mm, width of 12.5 mm, and thickness of 5 mm. Both molded and 3D printed specimens were lightly sanded before testing to remove sharp edges or surface defects. A TestResources 50 kN test machine, equipped with a 3-point bending fixture, was employed for flexural loading at a rate of 1.3 mm min^{-1} until failure. The supports were placed symmetrically beneath the rectangular specimens with a span of 47 mm. During testing, load-displacement curves were acquired, and the flexural strain (ϵ) and stress (σ) were calculated with Eq. [1] and [2], respectively:

$$\epsilon = \frac{6Dd}{L^2} \quad [1]$$

$$\sigma = \frac{3PL}{2bd^2} \quad [2]$$

Where,
D = cross-head displacement (mm);
d = specimen's thickness (mm);
L = span length (mm);
P = applied load (N); and
b = specimen's width (mm).

Each experiment was carried out on six to eight specimens (n = 6 to 8) for each molded and printed geometry. To remove any outliers, the Chauvenet's Criterion method was used when analyzing all data.

Figure 4. Mold geometries for (a) tensile test specimens and (b) 3-point bending specimens, (c) molded dogbone specimen during tensile testing, and (d) 3D printed specimens for 3-point bending in the longitudinal and transverse directions [29]

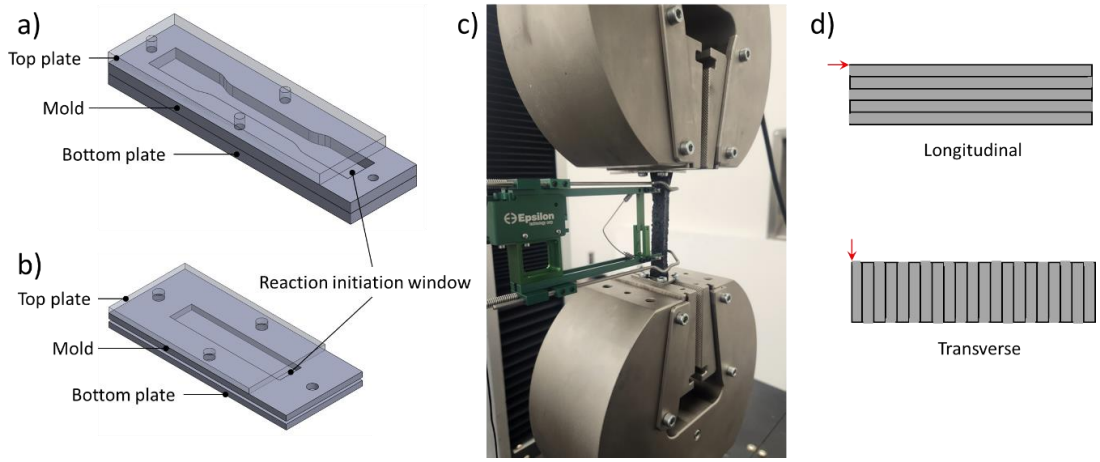

Discussion of Results

In this report, results will be presented for each polymer composite system separately, then compared in the Conclusions and Recommendations sections.

Frontal Polymerization Resin and 3D Printing

Rheological behavior

A study of the rheological properties of the printing resin containing different FS and CNF loadings was performed. An expected increase in viscosity was seen with increasing fumed silica and carbon nanofiber in the profiles presented in Figure 5. The viscosity decreased with increasing shear rate, indicating that the filled resin possesses shear thinning behavior, which is beneficial to extrusion-based 3D printing. Similar epoxy resins containing fumed silica meant for frontal polymerization have been found to exhibit shear thinning behavior, where viscosity decreases with an increase of shear strain or shear rate [33]. The unfilled printing resin did not appear to exhibit the same properties. Instead, its viscosity remained relatively constant when shear rate increased. Outcomes from previous work on extrusion-based AM of thermosets suggested that the viscosity range obtained for resin formulations containing at least 2 wt% FS and 2 wt% CNF could be high enough to maintain filament dimensional stability after deposition [18,34].

Figure 5. Viscosity profiles from steady-state shear experiments showing the effect of shear rate on the rheological behavior of the FP resin containing different weight fractions of fumed silica (FS) and carbon nanofiber (CNF) [29].

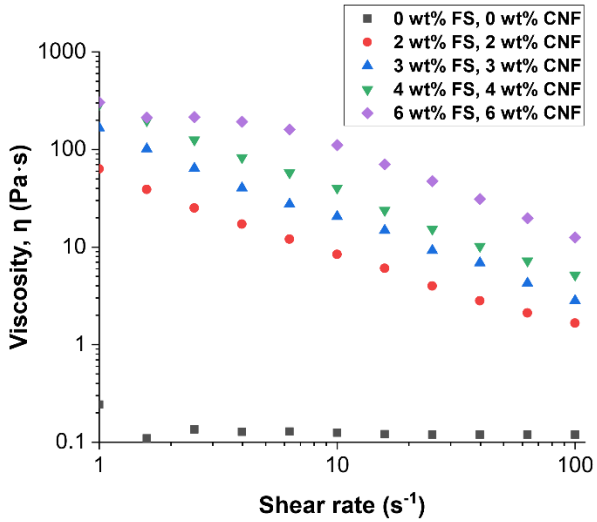

Parametric study on composite formulations

To enable free-standing printing, the resin must be viscous enough to limit sagging as it is extruded, and the nozzle speed must be coordinated with the front speed to obtain solidification close to the tip while avoiding clogging. For the extrusion and printing studies, resin formulations containing between 2 wt% and 4 wt% FS and CNF were investigated because they possessed suitable viscosity. Viscosity is a critical parameter in 3D printing, influencing the flow behavior of the resin during extrusion and the layering process. As summarized in Figure 5, adding fillers to the resin affected its rheological properties. It was experimentally observed that beyond a certain concentration (> 4 wt% FS and 4 wt% CNF), the high resin viscosity made it challenging to extrude and print the material with consistent flow (above approximately 288 to 5.2 Pa·s, from 1 s^{-1} to 100 s^{-1} shear rate). This resulted in issues, such as nozzle clogging, uneven layer deposition, and poor print quality. Therefore, a range of filler weight fractions from 2 wt% to 4 wt% was chosen for the parametric studies.

Figure 6 shows a summary of preliminary extrusion experiments to find suitable pressure and printing speed ranges for extrusion of the resin containing FS and CNF. Figure 6a compares extruded filaments under pressures from 0.02 to 0.15 MPa for two nozzle diameters and two resin formulations. The filament exhibited smoother and more consistent behavior as pressure and nozzle diameter increased. While the extrusion was

consistent for the lowest FS and CNF weight fractions (2 wt%), it was observed that the viscosity was too low to ensure the filament would retain its shape after extrusion and deposition (a range from approximately 1.7 to 63 Pa·s, depending on shear rate, as seen in Figure 5). This was noted for 3 wt% formulations as well, confirming that 4 wt% would be the most suitable for free-standing 3D printing. From the rheological measurements (Figure 5), the 4 wt% formulation corresponds to a viscosity range from 5.2 to 288 Pa·s at a shear rate of 100 s^{-1} to 1 s^{-1}. Assuming pipe flow in the nozzle and a flow rate consistent with the printing speed (1.5 to 6 cm min^{-1}), the actual shear rate at the nozzle is estimated between 0.13 s^{-1} and 0.5 s^{-1}. 29 By fitting the data points presented in Figure 5 with a power law function, the extrapolated viscosity at the actual shear rates in the printing process varies between approximately 1790 and 540 Pa·s.

The 4 wt% resin formulation was then used to extrude single filaments under 0.02 MPa pressure at different printing speeds (from 1.5 to 6 cm min^{-1}, a value close to the front velocity of 5.6 to 6.3 cm min^{-1}) to identify a suitable range producing filaments with consistent width and thickness, while matching the front velocity of the resin system. The results are presented in Figure 6b, confirming that filament width and thickness decreased with low standard deviation, as the speed increased up to 6 cm min^{-1}. This indicates that using the 4 wt% resin formulation, in combination with a nozzle diameter of 2 mm and a pressure of 0.02 MPa, could be suitable for free-standing printing as it would be possible to coordinate front and printing speeds. Using a higher pressure would require a higher printing speed to maintain consistent filament extrusion, but could exceed the front velocity, leading to filament sagging and unsuccessful free-standing printing.

Figure 6. (a) Comparison of extruded filament at syringe tip for different pressures, nozzle diameters, and resin formulations, and (b) Effect of printing speed on deposited filament width and thickness for 4 wt% FS, 4 wt% CNF formulation with 2 mm diameter nozzle and under 0.02 MPa pressure. Top views of the deposited filaments are shown in inset in (b) for low and high printing speeds.

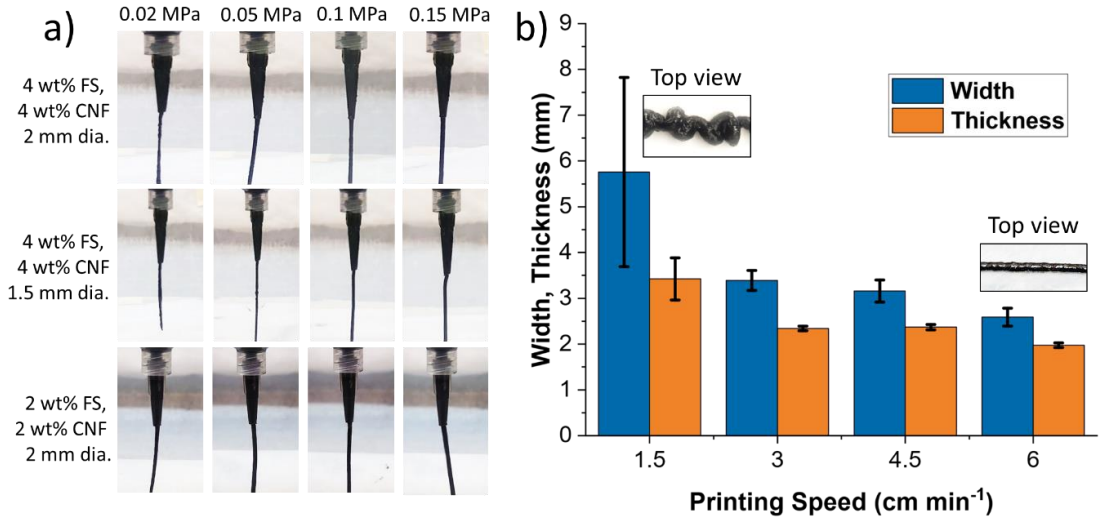

Mechanical characterization of composite specimens

The effect of FS and CNF weight fractions on the tensile properties of the resin system, for as-molded specimens, is shown in Figure 7a. The average ultimate strength increased with filler weight fraction, indicating effective reinforcement of the specimens. Similarly, the elastic modulus showed a slight increase as the filler loading increased from 2 wt% to 4 wt%. The strain at break confirmed rigid, brittle behavior of the resin system at all weight fractions. However, the large standard deviations for strain at break values imply the differences are not significant. The variations between specimens were likely caused by the porous nature of the resin system after frontal polymerization. Void formation in radical-induced cationic frontal polymerization (RICFP) systems has been previously reported and is caused by the decomposition of the initiators producing gas [30]. Voids were present in the fractured surfaces and on the specimens' surface, potentially creating damage initiation sites. Overall, it is expected that variations in tensile properties mostly depend on the presence of voids. In the literature, tensile properties of RICFP-cured epoxies without and with different fillers (woven carbon fiber plies [31], multiwalled carbon nanotubes (MWCNTs) [17], or continuous carbon fibers [26]) were reported. Printed composite specimens containing 1 wt% MWCNT exhibited tensile strength in the same order of magnitude as formulations in Figure 7a [26]. Reinforcing material and architecture (woven, continuous carbon fibers) significantly increased elastic modulus and tensile strength [17,26,31], but generally, comparable or higher front velocities were obtained with our 4 wt% formulation (above 5 cm min^{-1}).

The influence of manufacturing approach on the flexural behavior of composite specimens was assessed through 3-point bending. Figure 7b compares the flexural strength of molded specimens and 3D printed specimens in the longitudinal and transverse directions. It shows that molded specimens possessed the highest strength, followed by 3D printed specimens in the longitudinal, then transverse directions. It is expected that the molded specimens displayed the highest strength because the fabrication process involved compression of the specimen between two acrylic sheets. This created more even front propagation and surfaces, compared to 3D printed specimens, for which the bottom surface in contact with the printing bed exhibited a more porous morphology. The reduced strength for 3D printed specimens may be further attributed to adhesion issues between adjacent filaments and possible defects introduced by voids, especially for those printed in the transverse direction. The lowest strength in the transverse direction could also be explained by preferential CNF alignment along the

extruded filaments, leading to lower flexural properties compared to the longitudinal direction, as suggested in the literature for different frontal polymerization systems [32].

Figure 7. (a) Comparison of tensile properties for as-molded FP resin specimens with increasing FS and CNF percentage, and (b) comparison of flexural strength for FP resin specimens (4 wt% FS, 4 wt% CNF) as-molded, and 3D printed in the longitudinal and transverse directions [29].

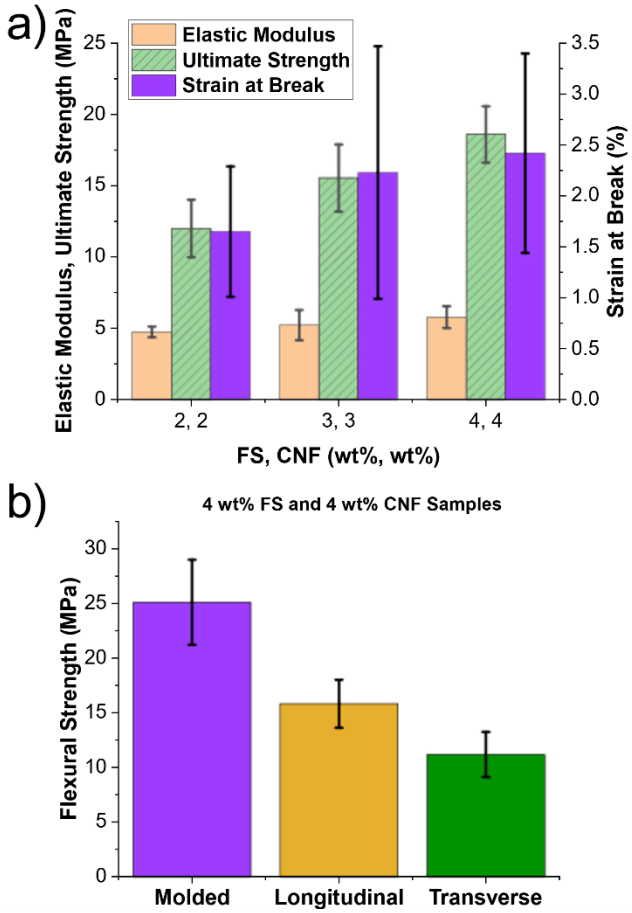

Free-standing AM demonstration

Figure 8 shows different 3D printing geometries to assess feasibility of printing approaches. Layer-by-layer cylindrical geometries were first 3D printed (Figure 8a) to assess main issues. Initially, coordination between front velocity and extruder speed was attempted by selecting a printing speed of 6 cm min^{-1}. However, as layers were deposited on top of existing layers, which were still at high temperature, the front propagation was initiated at the syringe tip, clogging the extruder. To avoid this issue, a higher printing speed between 40 cm min^{-1} and 45 cm min^{-1} was used, which allowed successful fabrication of the planar specimen.

For free-standing printing, the main challenge was to achieve solidification of the filament as it is extruded by maintaining adequate distance between nozzle and front. A print speed that closely matches the front velocity is optimal for this process. Several trials were performed to study the effect of reaction initiation with a soldering iron and printing speed. Single filaments were extruded at a 40º angle at printing speeds between 5.0 cm min^{-1} and 5.5 cm min^{-1}, as shown in Figure 8e. Figure 8e-i and Figure 8e-ii compare different reaction initiation delays at the same printing speed. A longer reaction initiation delay, where the distance between the nozzle and the front was above 10 mm, led to a specimen geometry and angle significantly deviating from the planned path at 40º. A printing speed of 5.2 cm min^{-1} (Figure 8e-iii and Figure 8e-iv) with a reaction initiation delay between approximately 5 mm and 7 mm allowed free-standing printing of filaments with angles between 38º ± 2º and 40º ± 2º. However, as the reaction initiation method required contact with the filament upon extrusion, the base of the filaments was inconsistent. Finally, a higher printing speed of 5.5 cm min^{-1}, along with a reaction initiation delay lower than 5 mm, showed a curved filament shape. This indicates the reaction was initially well-coordinated with the nozzle, but the distance between nozzle and front increased over time, due to the printing speed. From those initial trials, a printing speed of 5.2 cm min^{-1} was selected, and the reaction initiation method was improved by using two UV spotlights to eliminate physical contact. Helical geometries were then manufactured to demonstrate feasibility of free-standing 3D printing with the proposed resin system (Figure 8b to d).

Ongoing work addresses void formation during frontal polymerization to create structures with higher dimensional stability and mechanical performance. Depending on printed geometry, print speed must be adjusted to prevent front propagation between layers, which would lead to failure of the print. This is shown with the significant differences between print speeds of free-standing helical and layered cylindrical structures.

Figure 8. (a) 3D printed planar, cylindrical specimen, (b) and (c) examples of free-standing helical filaments during extrusion, (d) helical specimen from (c) after extrusion, and (e) free-standing filaments at a 40˚ angle at different printing speeds and reaction initiation delays [29].

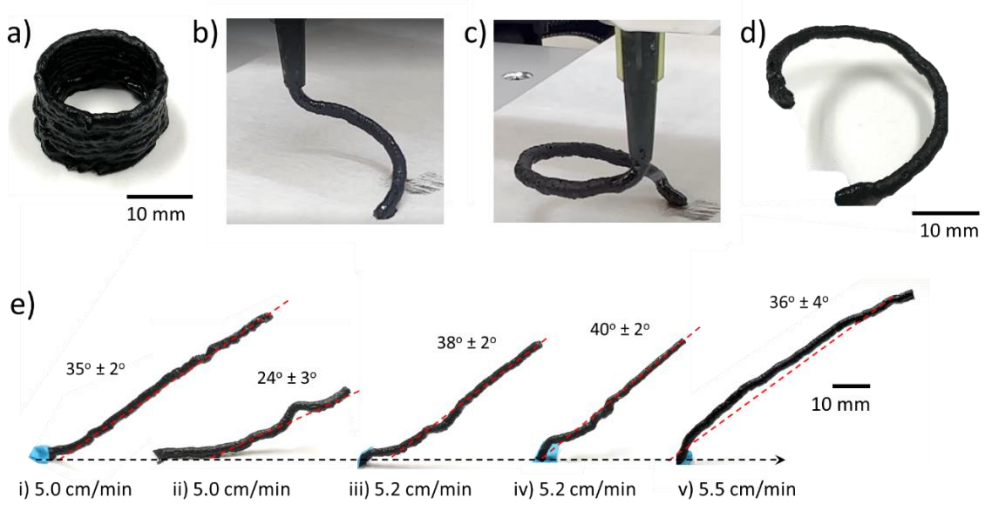

GF/Photopolymer and 3D Printing

Desktop 3D printing setup

Figure 9 shows examples of free-standing truss structures printed with the desktop system. Through initial trials, it was found that a printing speed of 10 mm/s (60 cm min^{-1}) with two UV lights (100 % intensity, 5.6 W cm^{-2} at a distance of 13 mm) allowed sufficient solidification of the photopolymer as it is extruded. While this is a faster speed than the FP resin, the photopolymer specimens would still need to be post-cured via UV light to achieve full solidification (duration varies based on size, but from 2 minutes up to ~15 minutes). However, with this setup, a fundamental issue was identified when trying to manufacture free-standing truss geometries. Due to the fixed extruder and syringe tip (only XYZ movement allowed, but no rotation), it was not possible to print the whole structure in one step as the extruder head would come into contact with the sections that had already been printed and solidified. To circumvent this issue, two options were considered: 1) re-designing the extruder head to increase the nozzle length or 2) printing truss sections separately, from bottom-up. The first option was judged impractical as nozzle length could lead to inconsistent resin flow and UV lights attachment would be impractical (as lights need to be close to the nozzle tip to insure sufficient curing). Therefore, the second option was employed to maintain the free-form nature of the print

(instead of printing a planar, triangular geometry on the print bed). Each truss section was sequentially extruded from bottom-up, as shown in Figure 9a (1, then 2). Figure 9b and Figure 9c illustrate the effect of pressure when increased from 0.04 MPa to 0.08 MPa, resulting in more consistent extrusion and dimensions. Mechanical characterization was not yet performed as the contact at the top of the truss structure is inconsistent. Overall, based on this setup limitations, a robotic arm system would enable more flexible extrusion of complex structures (seen in Figure 1) as the end-effector can be rotated/angled via a joint.

Figure 9. (a) Desktop 3D printing setup during photopolymer extrusion where each truss section is sequentially extruded from bottom-up (1, then 2), (b) and (c) examples of free-standing truss structures printed at 0.04 MPa and 0.08 MPa, respectively.

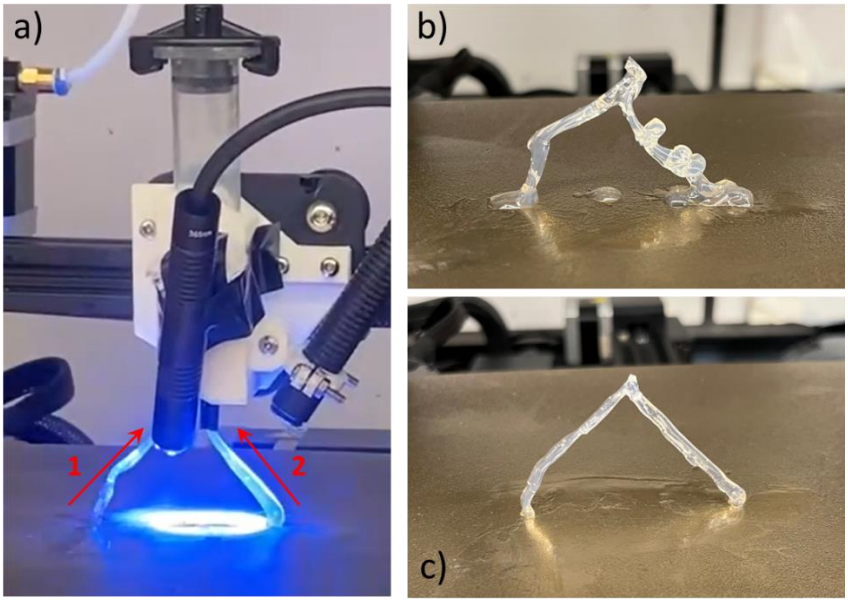

Robotic 3D printing demonstration

Figure 10 presents preliminary experimental results with the robotic 3D printing system developed for this project by a team of Capstone Design students. Initial 3D printing tests at constant pump speed (between 2.5% and 15%), roller tension, UV light intensity (75%), and arm velocity were performed with continuous glass fiber/photopolymer filaments.

Free-standing angled filaments and planar specimens (e.g., cylindrical geometries with 10 cm diameter) were printed to assess impregnation quality and curing capabilities without

the use of supports (Figure 10a and Figure 10b, respectively). Cross-sectional microscopy (Figure 10c) revealed generally uniform GF distribution within the extruded filaments, with a moderate void fraction. The addition of continuous GF increased stiffness of the structure during printing, compared to specimens in Figure 9, which can improve dimensional stability and performance. Overall, potential for free-standing printing of composite structures was demonstrated, which can be leveraged for complex structures, such as various bridge truss geometries.

Some issues were discovered during those experiments: 1) the fiber filament needs to be securely anchored before starting the print and 2) the impregnation chamber to combine GF and resin tends to get clogged easily if not regularly cleaned. This is a time-consuming process that could be facilitated by improving the chamber design moving forward. Moreover, during this project, a detailed manual was written to insure the next student(s) would be able to use this complex robotic system with limited downtime.

Additional studies are currently in progress, including quantification of void fraction, dimensions, and flexural stiffness. The quality of the printed samples could be further improved with utilization of the motor roller assembly which compresses the fibers before they pass through the impregnation chamber. In addition, further investigation of the effect of printing parameters to optimize print quality for different thermoset resins (pump pressure, roller tension, UV light intensity, and arm velocity) will be conducted.

Figure 10. Examples of GF/photopolymer structures printed with the robotic setup: (a) free-standing angled filament, (b) planar, cylindrical specimen, and (c) cross-sectional microscopy image of filament printed in (a).

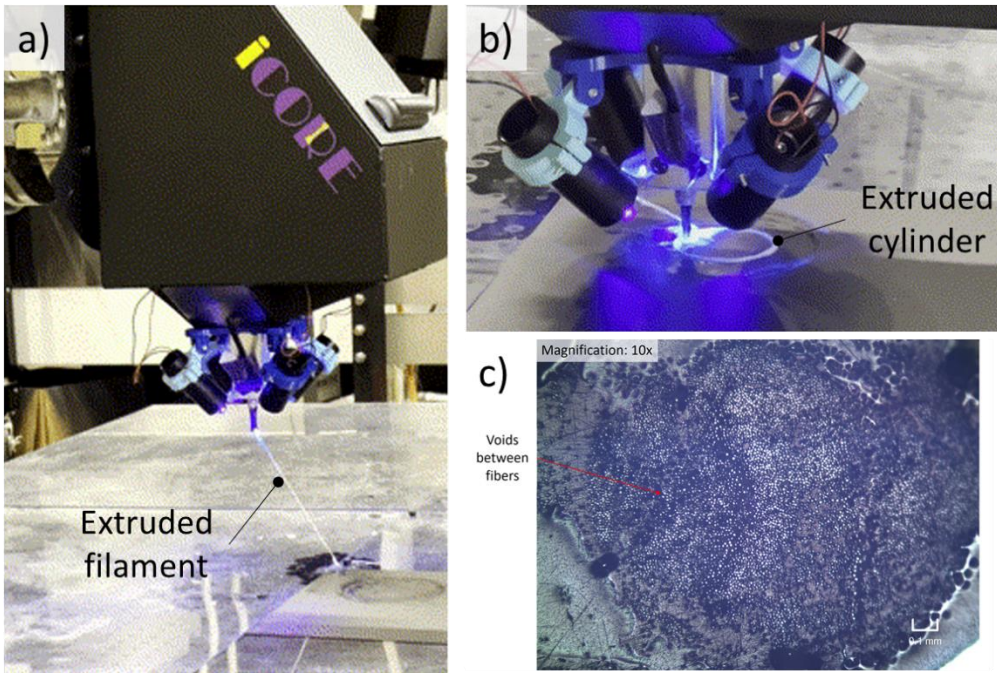

Conclusions

In this work, we studied two different polymer composite materials for free-standing 3D printing toward truss structures. First, a radical-induced cationic frontal polymerization resin was formulated with fillers (fumed silica and carbon nanofibers) to increase viscosity and limit sagging during extrusion at the nozzle tip. To demonstrate extrusion-based additive manufacturing, a desktop 3D printer was modified to control resin extrusion and deposition via a digital syringe dispenser. A parametric study compared the effect of air pressure, nozzle diameter, and filler weight fraction on extrusion behavior, revealing a formulation containing 4 wt% fumed silica and 4 wt% carbon nanofibers was the most suitable for free-standing printing. The main goal was to achieve a viscosity for consistent extrusion through the nozzle, while avoiding sagging of the extruded material at the nozzle tip. An air pressure of 0.02 MPa allowed extrusion of dimensionally stable filaments at a printing speed matching the front velocity (between 5 and 6 cm min^{-1}). Flexural properties of molded and 3D printed specimens were obtained through 3-point bending tests, showing specimens printed in the transverse direction exhibited the lowest strength. This is likely due to the presence of voids within and between filaments, adhesion issues, and preferential carbon nanofiber alignment along the filaments. Finally, free-standing printing was successfully demonstrated with single, angled filaments and helical geometries.

Second, a photopolymer was used to demonstrate potential for free-standing 3D printing. Fumed silica (8 wt%) was added to the resin for printability and two UV lights were employed to enable partial solidification during extrusion with the desktop 3D printer. While truss structures were successfully printed, the printing setup limited the complexity of the free-form geometries due to the fixed extruder head. A robotic 3D printing system was designed and manufactured with a custom extruder end-effector to facilitate free-standing printing of complex geometries. In this case, continuous GF tows were combined with the photopolymer via an in-situ impregnation chamber in the end-effector to produce filaments and structures with higher strength and stiffness. Free-standing angled filaments and planar, cylindrical specimens were successfully printed to assess quality and curing capabilities without the use of supports. Generally uniform GF distribution and moderate void fraction were achieved within the filaments. Overall, potential for free-standing printing of composite structures was demonstrated with the robotic system, which can be leveraged for complex structures, such as various bridge truss geometries.

Recommendations

The outcomes from this project revealed advantages and disadvantages for both materials studied. The FP resin formulation showed low mechanical performance, but it can be improved by reducing void content and incorporating fiber reinforcement. The photopolymer allowed faster 3D printing compared to the FP resin, but likely requires post-curing, which may be challenging for larger structures.

Further work is needed to fully characterize both material systems for potential bridge structures. For the FP resin, ongoing and future work focus on: 1) reduction of void formation, which would improve mechanical performance, and 2) reinforcement via continuous GF or CF tows (effect on front propagation speed, void characterization). For GF/photopolymers with the robotic 3D printing system, ongoing and future work focus on: 1) design of anchoring method before starting the print, 2) improvement of impregnation chamber to combine GF and resin for easier maintenance between experiments, 3) quantification of void fraction, dimensions, and flexural stiffness of printed filaments, and 4) effect of printing parameters to optimize print quality (pump pressure, roller tension, UV light intensity, and arm velocity). As the robotic 3D printing system is very complex to use, design changes and manufacturing steps will be documented in detail to insure smooth hand-off to the next student(s) working on this project.

Acronyms, Abbreviations, and Symbols

Term	Description
3PB	3-point bending
AASHTO	American Association of State Highway and Transportation Officials
AM	Additive manufacturing
BADGE	Bisphenol A diglycidyl ether
C3DP	Construction 3D printing
CAD	Computer-aided design
CE	3,4-epoxycyclohexylmethyl-3,4-epoxycyclohexanecarboxylate
CF	Carbon fiber
cm	Centimeter(s)
CNF	Carbon nanofiber
CNT	Carbon nanotube
DIW	Direct ink writing
FHWA	Federal Highway Administration
FP	Frontal polymerization
FRP	Fiber-reinforced polymer
FS	Fumed silica
GF	Glass fiber
kN	Kilo Newton
LTRC	Louisiana Transportation Research Center
mm	Millimeter(s)
min	Minute(s)
MPa	Megapascal(s)
MWCNT	Multiwalled carbon nanotube
nm	Nanometer(s)
Pa.s	Pascal.second
RICFP	Radical-induced cationic frontal polymerization
rpm	Rotation per minute
s	Second(s)

Term	Description
TEGDVE	Tri(ethylene glycol) divinyl ether
UV	Ultraviolet
W	Watt(s)
WAAM	Wire arc additive manufacturing
wt	Weight fraction

References

[1] National Bridge Inventory, U.S. Department of Transportation - Federal Highway Administration, 2022.

[2] B. Wan, 1 - Using fiber-reinforced polymer (FRP) composites in bridge construction and monitoring their performance: an overview, in: Advanced Composites in Bridge Construction and Repair, Woodhead Publishing, pp. 3-29, 2014.

[3] H. Baghi, F. Menkulasi, J. Parker, J.A.O. Barros, Development of a High-Performance Concrete Deck for Louisiana Movable Bridges: Numerical Study, Journal of Bridge Engineering, 22, 04017028, 2017.

[4] T. Ulger, A.M. Okeil, Effect of initial panel slenderness on efficiency of Strengthening-By-Stiffening using FRP for shear deficient steel beams, Thin-Walled Structures, 105, pp. 147-155, 2016.

[5] Standard Specification for Fiber-Reinforced Polymer Composite Materials for Highway and Bridge Structures, 2020.

[6] B.R. Groce, D.P. Gary, J.K. Cantrell, J.A. Pojman, Front velocity dependence on vinyl ether and initiator concentration in radical-induced cationic frontal polymerization of epoxies, Journal of Polymer Science, 59 (2021) 1678-1685.

[7] Z. Zhang, C. Gao, R. Liu, J. Qiu, Z. Pei, S. Wang, 3D Printing of Frontal-polymerized Multiscale Epoxy Thermoset and Composites, Manufacturing Letters, 33 (2022) 640-643.

[8] Y. Mizuno, N. Pardivala, B.L. Tai, Projected UV-resin curing for self-supported 3D printing, Manufacturing Letters, 18 (2018) 24-26.

[9] Z. Wynne, C. Buchanan, P. Kyvelou, L. Gardner, R. Kromanis, T. Stratford, T.P.S. Reynolds, Dynamic testing and analysis of the world's first metal 3D printed bridge, Case Studies in Construction Materials, 17 (2022) e01541.

[10] T. Wu, P. Jiang, X. Zhang, Y. Guo, Z. Ji, X. Jia, X. Wang, F. Zhou, W. Liu, Additively manufacturing high-performance bismaleimide architectures with ultraviolet-assisted direct ink writing, Materials & Design, 180 (2019) 107947.

[11] R. Abedin, X. Feng, J. Pojman, S. Ibekwe, P. Mensah, I. Warner, G. Li, A Thermoset Shape Memory Polymer-Based Syntactic Foam with Flame Retardancy and 3D Printability, ACS Applied Polymer Materials, 4 (2022) 1183-1195.

[12] R. Tu, H.A. Sodano, Additive manufacturing of high-performance vinyl ester resin via direct ink writing with UV-thermal dual curing, Additive Manufacturing, 46 (2021) 102180.

[13] K. Chen, X. Kuang, V. Li, G. Kang, H.J. Qi, Fabrication of tough epoxy with shape memory effects by UV-assisted direct-ink write printing, Soft Matter, 14 (2018) 1879-1886.

[14] R.D. Farahani, L.L. Lebel, D. Therriault, Processing parameters investigation for the fabrication of self-supported and freeform polymeric microstructures using ultraviolet-assisted three-dimensional printing, Journal of Micromechanics and Microengineering, 24 (2014) 055020.

[15] M. Asif, J.H. Lee, M.J. Lin-Yip, S. Chiang, A. Levaslot, T. Giffney, M. Ramezani, K.C. Aw, A new photopolymer extrusion 5-axis 3D printer, Additive Manufacturing, 23 (2018) 355-361.

[16] A.M. Abdullah, Y. Ding, X. He, M. Dunn, K. Yu, Direct-write 3D printing of UV-curable composites with continuous carbon fiber, Journal of Composite Materials, 57 (2022).

[17] Z. Zhang, R. Liu, W. Li, Y. Liu, H. Luo, L. Zeng, J. Qiu, S. Wang, Direct writing of continuous carbon fibers/epoxy thermoset composites with high-strength and low energy-consumption, Additive Manufacturing, 47 (2021) 102348.

[18] L. Velazquez, G. Palardy, C. Barbalata, A robotic 3D printer for UV-curable thermosets: dimensionality prediction using a data-driven approach, International Journal of Computer Integrated Manufacturing, (2023) 1-18.

[19] L. Velazquez, G. Palardy, C. Barbalata, Design and integration of end-effector extruder for 3D printing novel UV-curable shape memory polymers with a collaborative robotic system, in: CAMX 2021, Dallas, TX, 2021.

[20] B.A. Suslick, J. Hemmer, B.R. Groce, K.J. Stawiasz, P.H. Geubelle, G. Malucelli, A. Mariani, J.S. Moore, J.A. Pojman, N.R. Sottos, Frontal Polymerizations: From Chemical Perspectives to Macroscopic Properties and Applications, Chemical Reviews, 123 (2023) 3237-3298.

[21] J.A. Pojman, 4.38 - Frontal Polymerization, in: K. Matyjaszewski, M. Möller (Eds.) Polymer Science: A Comprehensive Reference, Elsevier, Amsterdam, 2012, pp. 957-980.

[22] N. Chechilo, N. Enikolopyan, Structure of the polymerization wave front and propagation mechanism of the polymerization reaction, in: Dokl. Phys. Chem, 1974, pp. 174-176.

[23] A. Mariani, S. Bidali, S. Fiori, M. Sangermano, G. Malucelli, R. Bongiovanni, A. Priola, UV-ignited frontal polymerization of an epoxy resin, Journal of Polymer Science Part A: Polymer Chemistry, 42 (2004) 2066-2072.

[24] B.R. Groce, D.P. Gary, J.K. Cantrell, J.A. Pojman, Front velocity dependence on vinyl ether and initiator concentration in radical-induced cationic frontal polymerization of epoxies, Journal of Polymer Science, 59 (2021) 1678-1685.

[25] Z. Zhang, R. Liu, W. Li, Y. Liu, H. Luo, L. Zeng, J. Qiu, S. Wang, Direct writing of continuous carbon fibers/epoxy thermoset composites with high-strength and low energy-consumption, Additive Manufacturing, 47 (2021) 102348.

[26] Z. Zhang, C. Gao, R. Liu, J. Qiu, Z. Pei, S. Wang, 3D Printing of Frontal-polymerized Multiscale Epoxy Thermoset and Composites, Manufacturing Letters, 33 (2022) 640-643.

[27] N. Hiremath, G. Bhat, 4 - High-performance carbon nanofibers and nanotubes, in: G. Bhat (Ed.) Structure and Properties of High-Performance Fibers, Woodhead Publishing, Oxford, 2017, pp. 79-109.

[28] Z. Zhang, C. Gao, R. Liu, W. Li, J. Qiu, S. Wang, Catalyzed frontal polymerization-aided 3D printing of epoxy thermosets, Additive Manufacturing Letters, 2 (2022) 100030.

[29] B.R. Groce, A.V. Aucoin, M.A. Ullah, J. DiCesare, C. Wingfield, J. Sardin, J.T. Harris, J.C. Nguyen, P. Raley, S.S. Stanley, G. Palardy, J.A. Pojman, Free-Standing 3D Printing of Epoxy-Vinyl Ether Structures Using Radical-Induced Cationic Frontal Polymerization, ACS Applied Polymer Materials, 6 (2024) 572-582.

[30] Y. Ma, Z. Liu, X. Qian, Y. Zhao, M. Li, P. Li, Effect of Excessive Iodonium Salts on the Properties of Radical-Induced Cationic Frontal Polymerization (RICFP) of Epoxy Resin, Industrial & Engineering Chemistry Research, 62 (2023) 4896-4904.

[31] M. Sangermano, I. Antonazzo, L. Sisca, M. Carello, Photoinduced cationic frontal polymerization of epoxy–carbon fibre composites, Polymer International, 68 (2019) 1662-1665.

[32] M. Ziaee, J.W. Johnson, M. Yourdkhani, 3D Printing of Short-Carbon-Fiber-Reinforced Thermoset Polymer Composites via Frontal Polymerization, ACS Applied Materials & Interfaces, 14 (2022) 16694-16702.

[33] B.R. Groce, E.E. Lane, D.P. Gary, D.T. Ngo, D.T. Ngo, F. Shaon, J.A. Belgodere, J.A. Pojman, Kinetic and Chemical Effects of Clays and Other Fillers in the Preparation of Epoxy–Vinyl Ether Composites Using Radical-Induced Cationic Frontal Polymerization, ACS Applied Materials & Interfaces, 15 (2023) 19403-19413.

[34] B. Wang, K.F. Arias, Z. Zhang, Y. Liu, Z. Jiang, H.-J. Sue, N. Currie-Gregg, S. Bouslog, Z. Pei, S. Wang, 3D printing of in-situ curing thermally insulated thermosets, Manufacturing Letters, 21 (2019) 1-6.